Numerical investigation of impacting water drops in air cross-flow

A. Criscione*, R. Röhrig, L. Opfer, I. Roisman and S. Jakirlić
Institute of Fluid Mechanics and Aerodynamics, Technische Universität Darmstadt,
Petersenstraße 32, 64287 Darmstadt, Germany

Abstract

A numerical investigation of the impact of a water drop on a solid surface in air cross-flow is carried out. For the numerical simulations a multiphase solver implemented into the open source CFD software package OpenFOAM is used, tracking and locating the free surface with the Volume-of-Fluid (VOF) technique. The results are experimentally validated exhibiting very good qualitative and quantitative agreement. This work represents an introductory study relevant to the formation of airframe icing resulting from the impact of Supercooled-Large-Droplets (SLD) onto the wings of aircrafts.

Introduction

Liquid drops appear in a variety of industrial processes as well as in everyday life and nature. Whether they are droplets dripping from the water tap, rain drops splashing onto the windshield of an automobile or aerosol paint jetting out of a spray gun, most of them have one thing in common: they interact with a solid surface. A proper insight of the interaction between droplet and solid surface is desired for many technical and engineering applications in order to control or improve processes. The normal impact of a liquid drop onto a solid surface is investigated to a great extent and widely understood [1, 2], whereas the impingement influenced by an air cross-flow acting onto the droplet is mainly unexplored.

In this regard, the impact of SLD onto an aircraft wing during the flight represents a dangerous phenomenon for the safety. This issue results from the possible formation of rime and glaze ice on the wings influencing to a large extend their aerodynamic properties. Rime ice forms under impact of small rain droplets ($D < 20\mu m$) at relatively low temperatures between -30$^\circ C$ and -10$^\circ C$. The drops freeze instantly, it means they freeze before spreading over the wing can occur. Accordingly, rime ice forms a rough, brittle and irregular layer over the contact surface. Glaze ice, however, develops after the impingement of larger and warmer drops of up to a few millimeters in diameter and temperatures between -10$^\circ C$ and 0$^\circ C$. In this regard, the supercooled drops freeze only partially while the remaining liquid continues to flow and spreads over the surface until it solidifies completely. Hence, glaze icing results in a smooth and solid layer [3].

The aforementioned phenomenon of wing icing occurs especially at leading edge but it might also lead to structural icing at the entire wing. The presence of such structural icing changes the aerodynamics and this is a very dangerous phenomenon which might cause e.g. the stalling of the wing. It additionally increases the aircraft weight modifing the flight dynamics of the airplane. In order to evaluate possible mechanisms or designs that minimize or prevent airframe icing, investigations of the physical processes behind the phenomenon are required. The present work about the drop impact under the conditions of air cross-flow represents an introductory study relevant to the glaze ice formation and propagation at the aircraft wing (the phase change due to icing is not presently considered).

Numerical Procedure

The numerical simulations are performed using a Finite-Volume-Method-based multiphase solver implemented into the open source package OpenFOAM. The solver is designed for two-phase flows of incompressible, isothermal immiscible fluids. The free surface is hereby represented using a VOF phase-fraction approach [4]. This method introduces an additional function γ, called the indicator function. It represents the fractional volume of fluid within one cell and ranges from 0 to 1. If a cell is filled entirely with fluid then $\gamma = 1$. If on the other hand the cell does not contain any fluid then $\gamma = 0$. This means that at the free surface γ has a value between 0 and 1 (Figure 1). Within this study the free surface itself is considered to be located at $\gamma = 0.5$ which represents the arithmetic mean value of the indicator function range. The transport equation for γ is calculated as follows:

$$\frac{\partial \gamma}{\partial t} + \nabla \cdot (\gamma U) = 0. \tag{1}$$

*Corresponding author: a.criscione@sla.tu-darmstadt.de

The curvature of the surface κ follows the divergence of the unit vector normal to the interface to

$$\kappa = -\nabla \cdot \left(\frac{\nabla \gamma}{|\nabla \gamma|} \right). \tag{2}$$

The coupling between pressure and velocity is hereby accomplished using the Pressure-Implicit-with-Splitting-of-Operators (PISO) algorithm for transient flows [5]. The applied solver is capable of running laminar and turbulent simulations, where all classes of turbulence models can be selected. In addition to this, different contact angle models, i.e. static and dynamic approaches, can be applied. A static contact angle model assumes a constant angle throughout the simulation, whereas the dynamic models are functions of instantaneous flow quantities such as the contact line velocity.

For modeling the impact of a water drop in air cross-flow, a boundary layer with a free stream velocity U_∞ over a flat plate must be initially generated. The droplet is then placed inside the flow field with an initial drop diameter D_0 and an initial velocity normal to the plate U_0. The distance between the wall and the starting position of the falling drop amounts to three drop diameters in order to allow for deformation of the drop caused by the cross-flow prior to the impact. It corresponds to approximately eight boundary layer thicknesses.

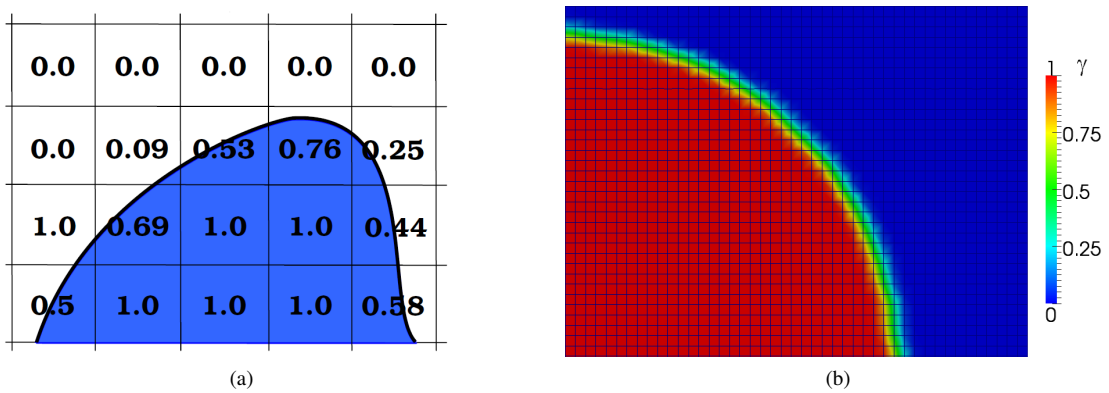

(a) (b)

Figure 1: (a) Schematic illustration of the VOF method [6]. (b) Close-up of the free interface region.

A crucial part of the numerical procedure is the generation of an appropriate computational mesh. Handling free surface flow and cross-flow within a continous numerical domain demands comparatively large overall dimensions as well as high spatial resolution. This results in a large number of volume cells, taking into consideration the three-dimensional character of the present flow problem. Furthermore, the flow is disturbed by the drop-induced vortices, which accelerate and decelerate the flow at certain points around the drop. The boundaries of the domain have to be located at regions where the flow is undisturbed, otherwise they might create an erroneous "boundary flow" leading to incorrect quantities inside the flow field as well as divergence of the computation. Since the regions of disturbed flow are fairly large in comparison to the drop diameter, the considered solution domain reaches comparatively large overall dimensions (Figure 2a).

The block structured mesh consists of differently refined sections as well as an uniformly refined wall layer (Figure 2b). The finest regions of the numerical domain are (1) the region in which the drop impacts, spreads and recedes and (2) the wall boundary layer. The smallest cell length is about $15\,\mu m$ which corresponds to approximately 66 cells per radius. Hexahedral grid cells are used due to their robustness regarding the two-phase flow, except for the transition of two differently refined regions. Here polyhedral cells and pyramids are employed in order to capture the connectivity areas adequately. It can be seen in Figure 2b, at the beginning of the simulation the droplet is located in a region in which the mesh is not as fine as at the impingement zone. Furthermore, the region in which the drop initially starts to fall is also coarser meshed then the two finest regions, otherwise the total number of cells would exceed the limit of an economic computational time. Due to symmetry reasons only the half of a drop (in the spanwise direction, Figure 2) is taking into consideration in the simulations. The final mesh used in this research consists of a total number of about $N = 5 \cdot 10^6$ volume cells.

The determining parameters in the field of the drop impact are the Reynolds number, $Re_0 = D_0\, U_0/\nu$, and the Weber number, $We_0 = \rho\, D_0\, {U_0}^2/\sigma$, where D_0 and U_0 are the initial drop diameter and the impact velocity and ρ, ν and σ are the liquid density, kinematic viscosity and surface tension, respectively. The numerical simulations and experiments are performed for an impacting drop with $Re_0 = 2000$ and $We_0 = 29$. The Weber number of

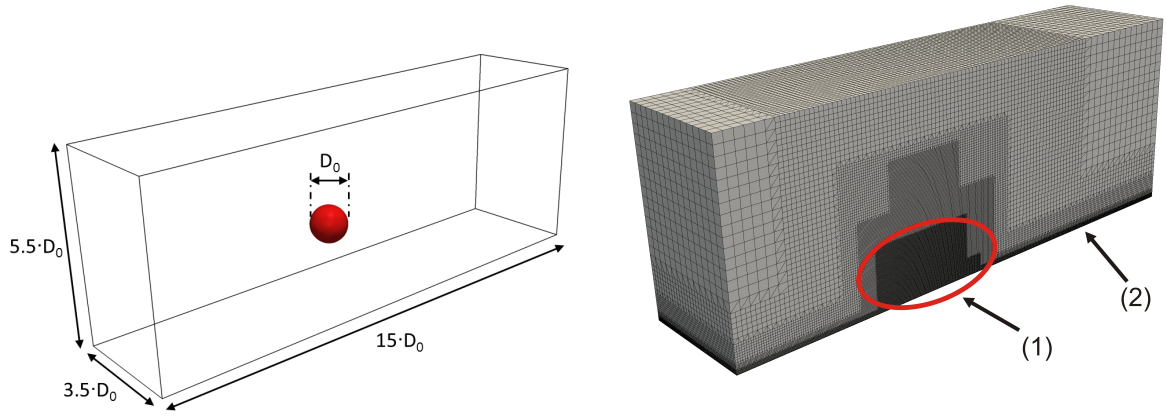

(a) (b)

Figure 2: (a) Outlined computational domain with its overall dimensions and the initial drop position. (b) Computational mesh in cell structure representation revealing the refinement in the drop and near-wall region.

the simulated cross-flow is defined as, $We = \rho_g \, D_0 \, {U_\infty}^2/\sigma$, where ρ_g represents the density of air and U_∞ the cross-flow velocity, is kept at $We \approx 3$, assuming a velocity of $U_\infty = 10\,m/s$. We, it is well below the critical Weber number of $We_{crit} \approx 11$ at which the so-called secondary atomization occurs [7]. The fluid properties used in the simulations are $\nu = 10^{-6}\,m^2/s$, $\rho = 10^3\,kg/m^3$ and $\sigma = 0.07\,N/m$ for the drop, $\nu_g = 1.48 \cdot 10^{-5}\,m^2/s$ and $\rho_g = 1\,kg/m^3$ for the cross-flow, where ν_g is the kinematic viscosity of the gas. These values correspond to water and air at a temperature of $T = 15°C$. The properties match the ones from the experiments.

Modeling of the contact angle

Several models describe the evolution of the contact angle of the fluid. One approach is to assign a constant value to the equilibrium contact angle Θ_e neglecting the contact angle hysteresis. This is also referred to as a static contact angle model. Using a constant contact angle, under the following assumption, $We_0 \gg 1$, yields quite accurate results for the spreading phase of the drop impact in which the lamella flow is inertia dominated, but not for the receding phase [8]. An alternative way is the application of a varying value of the angle between surface and impinging fluid, which depends on instantaneous flow parameters. These models are called dynamic contact angle models. One of the most recent and accurate ones is the Kistler model [9], which calculates the dynamic contact angle Θ_{dyn} using the Hoffman function f_{Hoff} as follows:

$$\Theta_{dyn} \;=\; f_{Hoff}\big[Ca + f_{Hoff}^{-1}(\Theta_e)\big], \tag{3}$$

where Θ_e is the equilibrium contact angle and $f_{Hoff}^{-1}(\bullet)$ the inverse of the function $f_{Hoff}(\bullet)$, which is defined as

$$f_{Hoff}(x) \;=\; arccos\left\{1 - 2\,tanh\left[5.16\left(\frac{x}{1+1.31x^{0.99}}\right)^{0.706}\right]\right\}. \tag{4}$$

The capillary number is defined as $Ca = U_{cl}\,\mu/\sigma$, where U_{cl}, μ and σ are the spreading velocity of the contact line, the dynamic viscosity of the liquid and the surface tension of the liquid and gas phase, respectively. Equation (3) shows that Θ_{dyn} depends significantly on the capillary number of the contact line and requires the input of an equilibrium contact angle. For surfaces which are not ideally smooth, i.e. which show a distinct contact angle hysteresis, the equilibrium angle Θ_e is replaced by either a limiting advancing or receding contact angle Θ_A or Θ_R, respectively, depending on the sign of the velocity vector at the contact line. Note that Θ_A and Θ_R are system properties that are determined from experiments [10].

Computational details

In the framework of this study the investigation of the drop impact in air cross-flow is performed for a drop Reynolds and Weber number of $Re_0 = 2000$ and $We_0 = 29$, respectively. The cross-flow velocity amounts

to $U_\infty = 10\,m/s$. The simulations are performed with both static and dynamic contact angle approaches. For the static model an equilibrium contact angle of $\Theta_e = 90^\circ$ is assumed, thus representing the contact angle of water on stainless steel as used in the experiment. For the dynamic model the Kistler approach is adopted with limiting advancing and receding contact angles measured experimentally. The flow within the wall boundary layer is assumed to be laminar as the relevant Reynolds number ($Re_x = U_\infty x/\nu$, where $x = 7.5D_0$) amounts to 10000, which is much smaller than the critical Reynolds number $Re_{crit} = 5 \cdot 10^5$. The simulation of the impact in cross-flow takes about 110 CPU-days on a *Intel Xeon E5472* processor which corresponds to one week of parallel computing on 16 cores.

Experiments

In order to validate the numerical results, complementary experiments are performed. They deal with droplet impacts under various cross-flow velocities and are analyzed both qualitatively and quantitatively. The experiments are carried out in a miniature wind tunnel which is specially designed for the purpose of investigating single drop impacts in air cross-flow. The tunnel is adjusted in size to droplets of diameters of the order of a few millimeters and is therefore comparatively small. The experimental setup is illustrated in Figure 3. The air cross-flow is generated by the fan of the wind tunnel (ii) which is steplessly adjustable by the potentiometer (vi). A syringe (iv) generates a drop outside the flow field. The droplet then falls down inside a tube and is thereby accelerated by gravity. Having reached a desired velocity after a given distance, it enters the flow field and eventually impacts onto a solid plate (v), that is placed inside the transparent test section of the wind tunnel. The impinging drop is captured by a high speed camera (iii) in the form of shadowgraph images under artificial lighting of a sodium-vapor lamp (i).

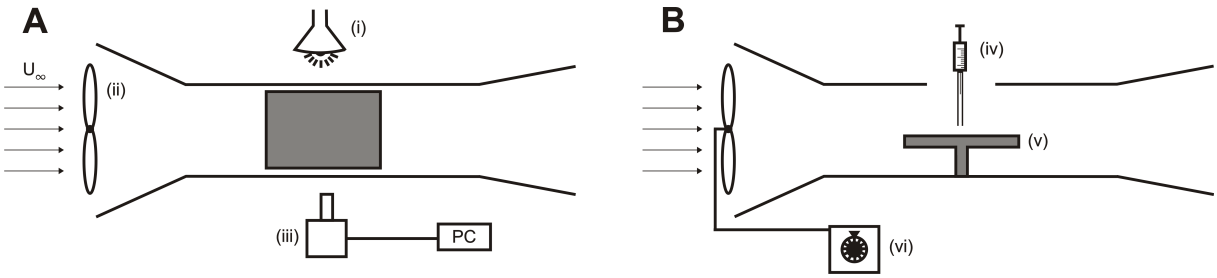

Figure 3: Experimental setup: top view **A** and side view **B**.

The experiments are carried out under the conditions of similarity in terms of Re_0 and We_0 with respect to the numerical computations. The spreading diameter of the contact line in streamwise direction, D_z, is extracted as the main quantity to be investigated.

Results

In the following, the numerical simulation of an impacting droplet in a cross-flow of $U_\infty = 10\,m/s$, applying the dynamic contact angle model according to Kistler, is compared to the corresponding wind tunnel experiment. In Figure 4 the qualitative comparison is shown. Snapshots from the experiment (upper figures) and the associated numerical results (lower figures) are illustrated. The advancing and receding contact angles for the Kistler model are $\Theta_A = 120^\circ$ and $\Theta_R = 45^\circ$, respectively, being selected to match the experimental conditions. The dimensionless time $\bar{\tau}$ is normalized according to $\bar{\tau} = t\,U_0/D_0$, where t represents the actual elapsed time.

The comparison between the experiment and the simulation as shown in Figure 4 reveals a good agreement. It is observed that the spreading phase is insignificantly influenced by the presence of the cross-flow, whereas the receding phase shows a distinct impact of the cross-flow onto the overall drop evolution. The quantitative results for the aforementioned comparison are plotted in Figure 5, where the evolution of the normalized spreading diameter, $\bar{D}_z$ ($= D_z/D_0$), is shown. In order to analyze the influence of the dynamic contact angle model, the results of the static contact angle computation are added to the plot.

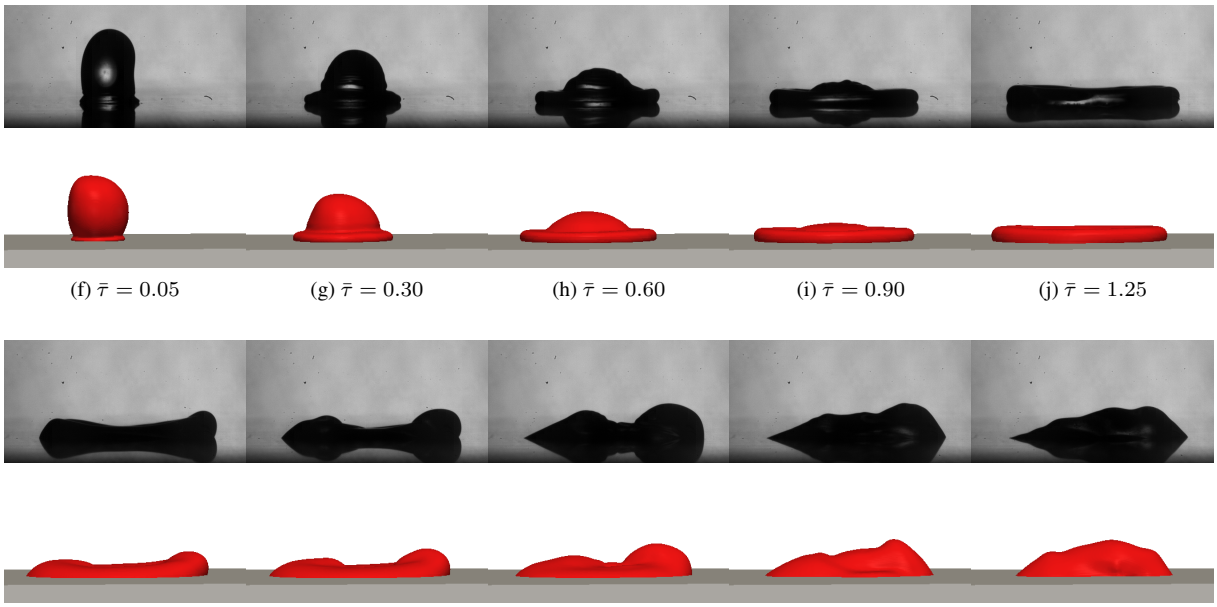

(f) $\bar{\tau} = 0.05$ (g) $\bar{\tau} = 0.30$ (h) $\bar{\tau} = 0.60$ (i) $\bar{\tau} = 0.90$ (j) $\bar{\tau} = 1.25$

(p) $\bar{\tau} = 2.30$ (q) $\bar{\tau} = 2.50$ (r) $\bar{\tau} = 2.95$ (s) $\bar{\tau} = 3.55$ (t) $\bar{\tau} = 4.05$

Figure 4: Qualitative comparison of a drop impact in air cross-flow of $U_\infty = 10\,m/s$: snapshots from experiments (upper figures) and corresponding numerical results (lower figures). Air cross-flow from the left.

It is observed that the Kistler model yields a remarkable improvement in matching the experimental results for an impacting drop at $U_\infty = 10\,m/s$. While the constant contact angle simulation results only in a qualitatively correct spreading diameter compared to the experiments, the results obtained appling the dynamic contact angle model exhibit a very good quantitative agreement. The dynamic approach reduces the maximum spreading diameter in accordance to the experiments. The same is valide for the slope of the diameter curve corresponding to the receding stage.

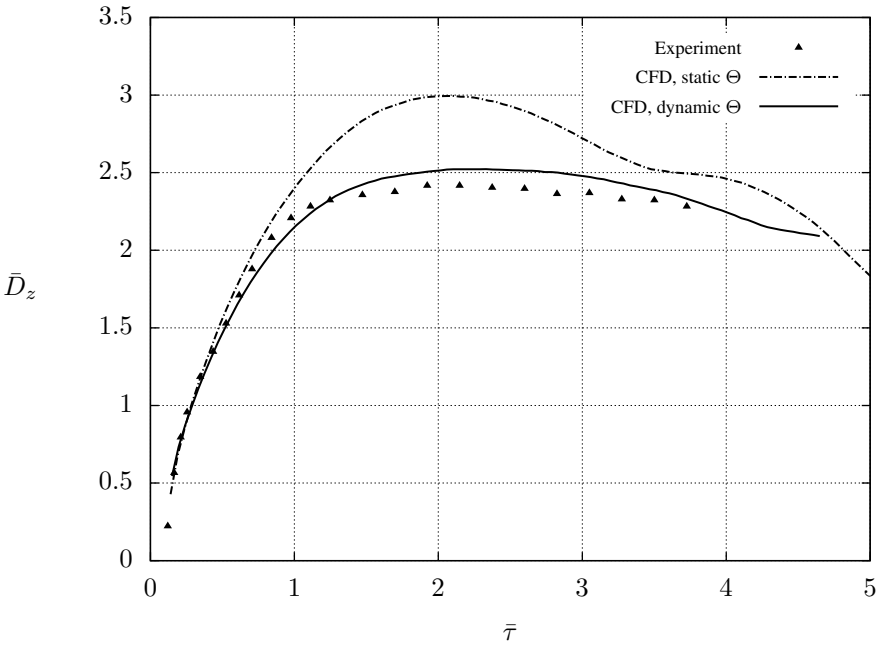

Figure 5: Comparison of numerical and experimental results for the spreading diameter, $\bar{D}_z$, with an air cross-flow velocity of $U_\infty = 10\,m/s$. Simulations are performed using a static contact angle $\Theta_e = 90°$ and the Kistler dynamic contact angle model.

Conclusions and outlook

The analysis of the numerical simulations and experiments shows that an air cross-flow of $U_\infty = 10\,m/s$ ($We \approx 3$) changes the impacting behavior of a droplet in the Weber number regime of $We_0 \sim \mathcal{O}(10)$. While the initial spreading phase of the drop is insignificantly influenced and reveals symmetric patterns, the subsequent spreading and receding phase shows a strongly asymmetric behavior with ellipsoidal shapes of the contact line. The outcome of the contact line is additionally influenced by drop deformation prior to the impact.

In the considered Weber number regime, the application performed in conjunction with the static contact angle model yielded non-satisfactory results for drop-wall-pairings that have a significant contact angle hysteresis. The dynamic contact angle approach according to Kistler [9], however, reveals a remarkably good matching between simulation and experiment with respect to the spreading diameter development and the drop shape evolution. The applied solver in combination with the Kistler contact angle model is thus considered to be advantageous for an impacting water droplet with air cross-flow.

Although numerical simulations of droplet impacts at cross-flow velocities of $10\,m/s$ were successfully performed and validated in this research, impacts at higher velocities remain to be investigated numerically. In this regard, Figure 6 shows the complexity of a so-called bag breakup as observed in further experiments at elevated air cross-flow velocity. The snapshots of this fascinating breakup structure brings up the even more fascinating question: "Is it possible to correctly capture this phenomenon within a numerical framework?".

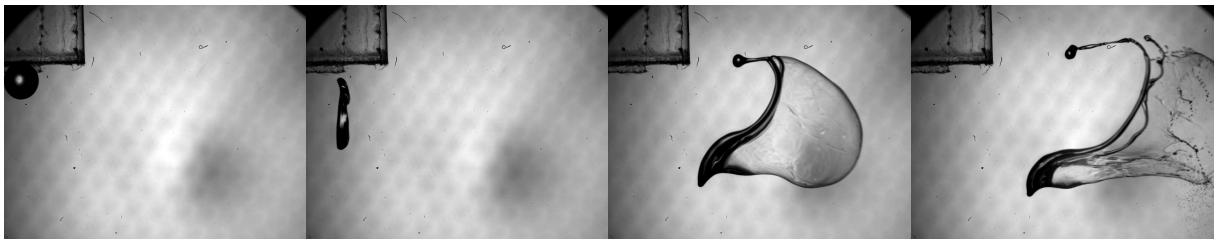

(a) $\bar{\tau} = 0$ (b) $\bar{\tau} = 1.50$ (c) $\bar{\tau} = 2.48$ (d) $\bar{\tau} = 2.71$

Figure 6: Water drop in an ambient flow field at elevated flow velocity ($U_\infty = 20\,m/s$) entering from the left.

Acknowledgments

This research was supported by the German Science Foundation (DFG) within the framework of the *SFB-TRR 75* program. The authors would like to thank R. Maduta and N. Linder for their technical and scientific support.

References

[1] Yarin, A.L., *Drop Impact Dynamics: Splashing, Spreading, Receding, Bouncing*. In: Annual Review of Fluid Mechanics 38:159-192 (2006).

[2] Roisman, I.V., Rioboo, R., and Tropea, C., *Normal impact of a liquid drop on a dry surface: model for spreading and receding*. In: Proceedings of the Royal Society A: Mathematical, Physical and Engineering Sciences, pp. 1411-1430 (2002).

[3] Bragg, M.B., *Rime ice accretion and its effect on airfoil performance*. Lewis Research Center, Report NAG3-28 (1982).

[4] Hirt, C., and Nichols, B., *Volume of fluid (VOF) method for the dynamics of free boundaries*. In: Journal of Computational Physics, 39:201-225 (1981).

[5] Issa, R.I., *Solution of the implicitly discretised fluid flow equations by operator-splitting*. In: Journal of Computational Physics, 62:40-65 (1986).

[6] Berberović, E., *Investigation of Free-surface Flow Associated with Drop Impact: Numerical Simulations and Theoretical Modeling*. PhD Thesis, Technische Universität Darmstadt (2010).

[7] Guildenbecher, D.R., López-Rivera, C., Sojka, P.E., *Secondary atomization*. In: Experiments in Fluids, 46:371-402 (2009).

[8] Šikalo, Š., Wilhelm, H.-D., Roisman, I.V., Jakirlić, S., Tropea, C., *Dynamic contact angle of spreading droplets: Experiments and simulations*. In: Physics of Fluids, 17, 062103 (2005).

[9] Kistler, S.F., *Hydrodynamics of wetting*. In: Berg, J.C. (Editor): *Wettability*, Marcel Dekker, New York, 1993.

[10] Roisman, I.V., Opfer, L., Tropea, C., Raessi, M., Mostaghimi, J., and Chandra, S., *Drop impact onto a dry surface: role of the dynamic contact angle*. In: Colloids and Surfaces A, Vol. 322, pp. 183-191 (2008).